Title

Ultralow Drive Voltage Substrate Removed GaAs/AlGaAs Electro-Optic Modulators at 1550 nm

Journal

IEEE Journal of Selected Topics in Quantum Electronics, 19(6)

ISSN

1077-260X

Authors

Shin, Jae Hyuk
Dagli, Nadir

Publication Date

2013

DOI

10.1109/jstqe.2013.2263122

Peer reviewed

Ultralow Drive Voltage Substrate Removed GaAs/AlGaAs Electro-Optic Modulators at 1550 nm

Jae Hyuk Shin, *Member, IEEE*, and Nadir Dagli, *Fellow, IEEE*

***Abstract*—This study reports ultralow drive voltage Mach–Zehnder modulators in highly confined substrate removed GaAs/AlGaAs optical guides with buried doped QW electrodes. Separation between the doped QW electrodes, which is the electrode gap, is only 0.15 μm. Such a small electrode gap results in very high electric fields overlapping very well with the optical mode. A careful analysis of the physical effects contributing to index change is presented and techniques to use these index changes efficiently are described. Fabrication details are given. Results of careful characterization of phase and Mach–Zehnder intensity modulators are presented. Variation of propagation loss and extinction ratio with applied voltage are investigated. Intensity modulators with 7-mm-long electrodes have 0.3 V V_π under push–pull operation with 15 dB extinction ratio. This corresponds to a 0.21 V·cm modulation efficiency in bulk compound semiconductors.**

***Index Terms*—Optical modulation, compound semiconductors, optical waveguides, phase modulation.**

I. Introduction

ELECTRO-OPTIC optical modulators are essential building blocks for any optical system. One of the most important properties of a modulator is the drive voltage also known as V_π. Many optical system properties such as drive power and link gain scale with the square of V_π. Hence, low V_π modulators are extremely important. At the present time most commonly used electro-optic modulators are $LiNbO_3$ based [1]. They have V_π of a few volts. Compound semiconductor modulators offer reduced V_π through enhanced phase-shift efficiency. Efforts to enhance phase shift efficiency of devices fabricated on bulk compound semiconductor material resulted in phase shift efficiency as high as 37.5 °/V·mm [2] at 1.3 μm and 27 °/V·mm [3] at 1.5 μm. These phase modulators utilized the high electrical field within the depletion region of a *pn*-junction to increase phase shift originating from the linear electro-optic (LEO) and quadratic electro-optic (QEO) effect. The depletion of charge also contributed to phase shift via plasma and band filling (BF) effects. More recently, QEO effects resulting from quantum confined stark effect (QCSE) in multiple quantum wells (MQWs) in InP- based material system were utilized to achieve high phase-shift efficiencies. Some of the reported MQW phase-shift efficiencies and the photoluminescence peaks, λ_{PL}, are 27.3 °/V-mm ($\lambda_{PL} = 1.37\mu$m) [4], 45 °/V·mm ($\lambda_{PL} = 1.414\,\mu$m) [5], 66.7 °/V·mm ($\lambda_{PL} = 1.45\,\mu$m) [6], 103.5 °/V·mm ($\lambda_{PL} = 1.47\,\mu$m) [7] all at the operating wavelength of 1.55 μm. As evident from these reports, QEO effect resulting from the QCSE is sensitive to wavelength and rapidly decreases as the operating wavelength moves away from the absorption edge of the structure. Therefore, the efficiency of modulators utilizing MQWs are sensitive to the amount of detuning of the operating wavelength from the photoluminescence peak. DC bias can be applied in addition to ac signal to overcome reduction in QEO effect [5] but the optical bandwidth is still limited to 30 nm. Moving closer to the absorption edge of the material also increases propagation loss due to material absorption. Therefore, the photoluminescence peak of the MQW must be carefully controlled.

In this paper, we improve upon the earlier results that were obtained from the bulk material by fabricating modulators on submicron thick epilayers removed from their growth substrates. These epilayers are glued onto another transfer substrate using a low-index polymer. This provides very high index contrast and modulator electrode gap can be made submicron. Studies in this direction have already resulted in Mach–Zehnder intensity modulators with 0.3 V V_π with only 7-mm-long electrode [8]. This paper describes a detailed description of such modulators and the issues that need to be addressed to realize them successfully.

The remainder of this paper is organized as follows. First, in Section II, the device description and design are presented. Next, in Section III, fabrication details are laid out, followed by measurement results and discussions in Section IV. Finally, a conclusion of the study is given in Section V.

Manuscript received March 1, 2013; revised April 27, 2013; accepted May 6, 2013. This work was supported in part by the National Science Foundation under Grants ECS-0501355 and 0702087.

J. Shin was with the Department of Electrical and Computer Engineering, University of California at Santa Barbara, Santa Barbara, CA 93106 USA. He is now with Aurrion, Inc., Goleta, CA 93117 USA (e-mail: jae.shin@aurrion.com).

N. Dagli is with the Department of Electrical and Computer Engineering, University of California at Santa Barbara, Santa Barbara, CA 93106 USA (e-mail: dagli@ ece.ucsb.edu).

Color versions of one or more of the figures in this paper are available online at http://ieeexplore.ieee.org.

Digital Object Identifier 10.1109/JSTQE.2013.2263122

II. Device Description and Design

In a push–pull driven Mach–Zehnder electro-optic modulator V_π is given as $V_\pi = (\lambda t) / \left(2Ln^3 r\Gamma\right)$. In this expression, L is the electrode length, λ is the operating wavelength, n is the mode effective index, r is the electro-optic coefficient, t is the electrode gap, and Γ is the overlap factor between the optical mode and externally applied modulating electric field. Once a material system and operating wavelength are chosen, the only parameters left for engineering are t, L, and Γ. The basic idea

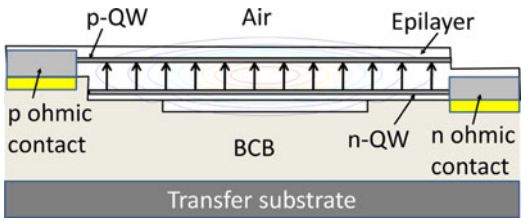

Fig. 1. Cross-sectional profile of a phase modulator formed in a substrate removed waveguide.

pursued in this study is to make Γ as large as possible and reduce t to submicron dimension, while keeping the propagation loss manageable so that a reasonably long L can be maintained.

This approach can be explained with the help of Fig. 1 which shows a phase modulator in a substrate removed waveguide. This waveguide is formed by removing a GaAs epilayer from its growth substrate and gluing it on top of a transfer substrate using benzocyclobutane (BCB). This figure also shows the intensity contours of the optical mode. As seen the mode can be confined very tightly in the vertical direction due to very high index steps. In this case, GaAs epilayer is only 0.3 μm thick. However electro-optical modulation requires external electrodes to apply the modulating electric field. This is normally achieved using metal electrodes, but in this case this approach is not acceptable. Even though the vertical optical confinement is very strong, mode still extends a submicron distance outside the epilayer. If metal electrodes are placed on both sides of the epilayer, metal overlaps strongly with the optical mode and optical propagation loss becomes excessively large. This makes the waveguide unsuitable for any practical application. We solve this difficulty by using buried electrodes made out of n- and p-doped quantum wells (QWs) as shown in Fig. 1. This forms a *p-i-n* diode in which the p and the n sides are contacted on the sides of the optical waveguide. Under reverse bias a very large electric field overlapping very well with the optical mode can be applied to the submicron i region. Since buried electrodes are contacted on the sides of the optical waveguide, the ohmic contacts and the contact metals do not overlap with the optical mode. There is some free carrier absorption loss due to doped buried electrodes. But having free carriers confined within the QWs reduces the overlap of the free carriers with the optical mode hence keeps the free carrier absorption loss minimal. In this case the electrode gap is the separation between the n and p doped QWs. This separation, which is the gap of the modulator electrode, can be made very small and uniform since it is determined by the material growth. We are able to reduce this gap to 0.15 μm with low propagation loss resulting in a practical device.

We also make intensity modulators using phase modulators of this type in the arms of a Mach–Zehnder interferometer. We tried several different approaches to fabricate such a waveguide. The difference is mainly in the formation of the rib region used for lateral confinement. The epitaxial layer details of the modulators fabricated are shown in Table I.

For all the devices, the first four layers above the substrate are etch stop layers used during substrate removal. These are not part of the device. All the layers are unintentionally doped

TABLE I
LAYER DETAILS OF THE MODULATORS FABRICATED IN THIS WORK

Device 1A Layers	Device 1B Layers	Device 2 Layers	Thickness (nm)
GaAs	GaAs	Si	60
$Al_{0.5}Ga_{0.5}As$	$Al_{0.5}Ga_{0.5}As$	$Al_{0.5}Ga_{0.5}As$	30
GaAs Be: $1.3x10^{18}cm^{-3}$	GaAs Si: $1.3x10^{18}cm^{-3}$	GaAs Si: $1.1x10^{18}cm^{-3}$	20
$Al_{0.5}Ga_{0.5}As$	$Al_{0.5}Ga_{0.5}As$	$Al_{0.5}Ga_{0.5}As$	15
GaAs	GaAs	GaAs	120
$Al_{0.5}Ga_{0.5}As$	$Al_{0.5}Ga_{0.5}As$	$Al_{0.5}Ga_{0.5}As$	15
GaAs Si: $1.3x10^{18}cm^{-3}$	GaAs Be: $1.3x10^{18}cm^{-3}$	GaAs C: $1.1x10^{18}cm^{-3}$	20
$Al_{0.5}Ga_{0.5}As$	$Al_{0.5}Ga_{0.5}As$	$Al_{0.5}Ga_{0.5}As$ C: $1.1x10^{18}$ cm^{-3}	30
GaAs	GaAs	GaAs	300
AlAs	AlAs	AlAs	200
GaAs	GaAs	GaAs	200
AlAs	AlAs	AlAs	200
GaAs substrate	GaAs substrate	GaAs substrate	-

except for the two GaAs QWs that are used as buried electrodes and the lower $Al_{0.5}Ga_{0.5}As$ barrier in device 2. In device 1 there were two epilayers in which the p and the n doping are switched. This changes the direction of the applied field and matters for the proper operation of the device as described later. The n and p doping were slightly lower in device 2. The only other main difference between devices 1 and 2 was in the top layer which is used for index loading to create lateral confinement. Device 2 uses a Si rib which confines the mode slightly better due to higher index of Si, whereas device 1's rib is GaAs. Fig. 2 shows the calculated energy band diagram of one of the designs we fabricated along with its secondary ion mass spectroscopy (SIMS) profile. Presence of two GaAs QWs and the charge in them are evident. It is also obvious that a very high electric field exists between these QWs and this field, and the charge in the QWs can be modified with an external voltage which creates refractive index changes. The refractive index of compound semiconductors can be changed utilizing several effects. These include LEO, QEO, PL, and BF effects. The theory of these effects in GaAs is well documented in [9]–[13]. The index change due to these effects can be written as follows:

$$\Delta n_{\mathrm{LEO}} = \pm\frac{1}{2}n^3 r E_y \tag{1}$$

$$\Delta n_{\mathrm{QEO}} = \frac{1}{2}n^3 A(\lambda) E_y^2 \tag{2}$$

$$\Delta n_{PL,N} = -9.6\times 10^{-21}\frac{\Delta N}{nE_p^2}$$

$$\Delta n_{PL,P} = -6.3\times 10^{-22}\frac{\Delta P}{E_p^2} - 1.8\times 10^{-21}\frac{\Delta P}{nE_p^2} \tag{3}$$

$$\Delta n_{B,N} = -B_N(\lambda)\Delta N \quad \Delta n_{B,P} = -B_P(\lambda)\Delta P \tag{4}$$

where n, r, and A are the refractive index, LEO and QEO coefficients of the material, E_y is the vertical electrical field, ΔN and ΔP are the change in electron and hole density, E_p is the

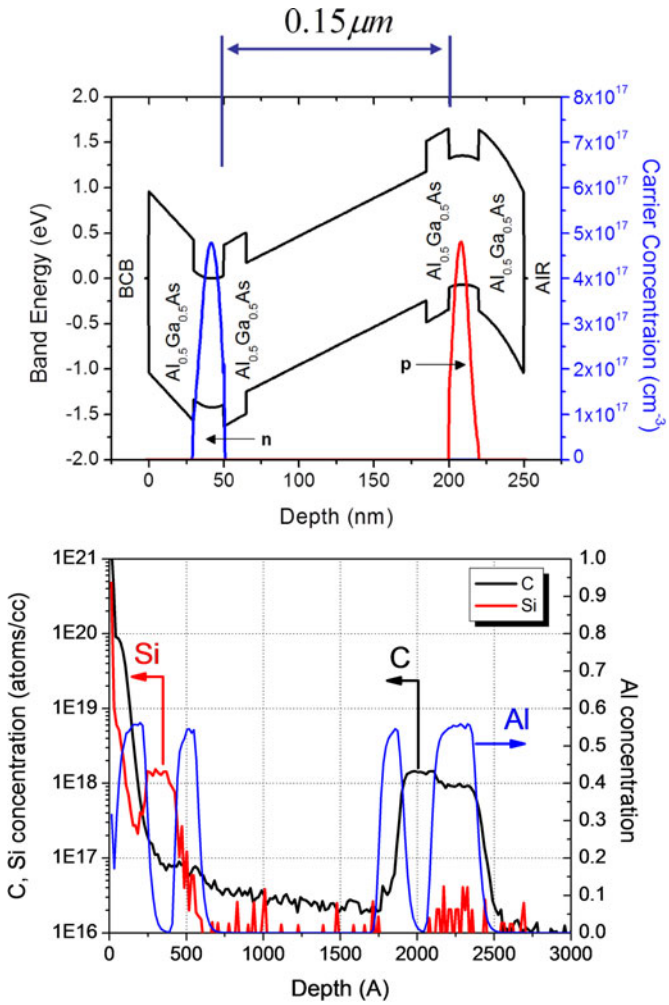

Fig. 2. Calculated energy band diagram and measured SIMS profile of one of the designs fabricated (device 2). The top layer was etched and is not observed both in the calculation and measurement.

photon energy, B_N and B_P are the BF coefficients for electrons and holes. The negative sign in front of the carrier related effects signify that the "removal" of charge increases refractive index. LEO effect can have either sign depending on the direction of E_y. The total phase shift due to these effects can be found using the following equation:

$$\Delta\Phi = \frac{2\pi L}{\lambda}\Delta n_{\text{eff}} = \frac{2\pi L}{\lambda}\sum_{i,j}\Delta n_{i,j}\Gamma_i \tag{5}$$

Here, n_{eff} is the mode effective index, λ is the free space wavelength, L is the electrode length, Γ_i is the overlap factor of the material experiencing index change with the optical mode. Subscript i labels regions with identical material and j labels the various effects (LEO, QEO, PL, and BF). The material parameters used in the calculation are tabulated in Table II [10]. All material parameters are well known except for the LEO coefficient of $Al_{0.5}Ga_{0.5}As$ which is linearly interpolated between the values of GaAs and AlAs. Since AlAs readily oxidizes in atmosphere, it is difficult to extract material coefficients. Since the band structure of GaP is very close to that of AlAs, we use the LEO coefficient of GaP [14] as that of AlAs.

TABLE II
MATERIAL PARAMETERS USED IN CALCULATIONS. $\lambda = 1.55\,\mu$m.

Material	Parameter	Value
GaAs	n	3.38
	r	1.50 x10^{-12} m/V
	A	7.72 x10^{-20} m^2/V^2
	B_N	1.47 x10^{-21} cm^{-3}
	B_P	0.42 x10^{-21} cm^{-3}
$Al_{0.5}Ga_{0.5}As$	n	3.13
	r	1.24 x10^{-12} m/V

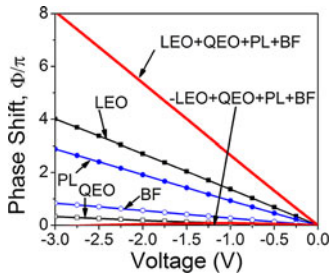

Fig. 3. Calculated phase shift as a function of voltage due to LEO, QEO, PL, and BF effects for devices 1A and 1B. Solid lines at the top and bottom without markers indicate the total phase shift when LEO either adds to or subtracts from the other effects, respectively. Electrode length is 1 cm.

In the calculations, a commercial semiconductor device solver called Atlas made by Silvaco and a commercial optical mode solver called mode solutions by Lumerical are used. Commercial semiconductor device solver generates carrier and electrical field profiles. Commercial optical mode solver generates the optical electric field. Results of these solvers are imported into MATLAB to find the various overlap factors and calculate the resulting effective index change. Finally effective index change is converted into the phase shift. Fig. 3 shows the phase shift calculations due to LEO, QEO, and free carrier related effects for devices 1A and 1B for 1-cm-long electrode.

We immediately see that even with a core thickness of 150 nm, QEO coefficient A is too small to contribute significant phase shift. LEO effect is still the most dominant contribution. The solid lines at the top and bottom without markers show the total phase shift when LEO effect adds to or subtracts from the other effects. When LEO effect subtracts from the others, they almost exactly cancel out. For device 1 the phase-shift efficiency when all effects add together is linear with voltage and has a slope of –2.68π/V·cm (48.2 °/V·mm), corresponding to a drive voltage length product of 0.37 V·cm for a push– pull driven Mach–Zehnder intensity modulator. The same value for device 2, which is not shown as a figure, is 0.3 V·cm. The difference is mainly due to slightly increased overlap factors arising from the higher index of Si used for lateral confinement.

III. DEVICE FABRICATION

The processing steps involved in the fabrication are shown in Fig. 4. These steps are for device 2. In this case, optical waveguides are defined by silicon lift-off based on electron beam lithography and evaporation. Next, the epilayer is etched

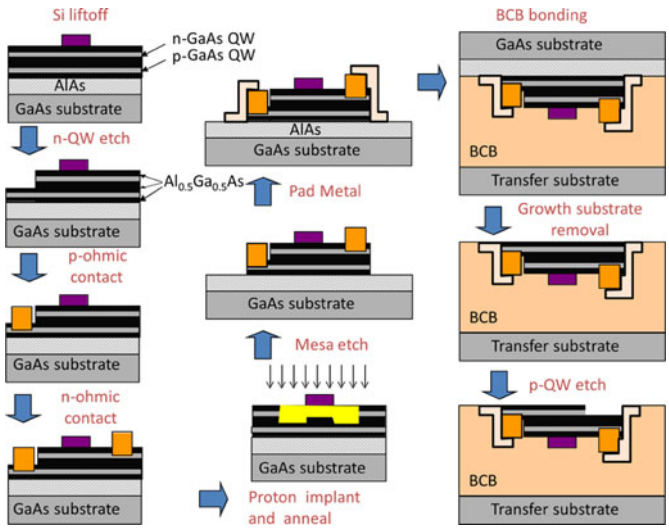

Fig. 4. Fabrication steps used in the fabrication of device 2.

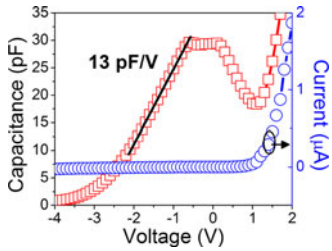

Fig. 5. *C–V* (open squares) and *I–V* (open circles) measurements of 7 mm phase modulator for device 1A.

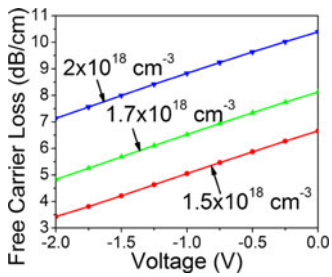

Fig. 6. Calculated free carrier absorption loss as a function of voltage for different QW doping levels.

midway into the GaAs core region with reactive ion etching with laser monitoring to gain access to the bottom QW. Following this step, Ti/Au (20/300 nm) is evaporated and lifted off for the p-ohmic contacts. After that Ni/AuGe/Ni/Au (5/150/20/300 nm) is evaporated and lifted off to form the n-ohmic contacts. Both contacts are annealed simultaneously at 430 °C for 2 min. Next, the device is capped with 100 nm SiO_2 to protect the surface from contamination. This is followed by H^+ implant performed at 150 keV. H^+ implantation is used to electrically isolate the arms of Mach–Zehnder interferometers. The implant is annealed at 340 °C for 30 s to recover some of the damage to prevent excessive optical loss. Next, the SiO_2 cap is removed in BHF. Mesa etch is performed with RIE to electrically isolate the devices. Ti/Pt/Au (20/40/800 nm) metal is evaporated and lifted off to form the contact pads. After cleaning the surface of the device with acetone, isopropyl alcohol, and deionized water, BCB is spun and partially cured to planarize the surface. Next, 50 nm Si_3N_4/160 nm SiO_2 is PECVD deposited on a separate semiinsulating GaAs wafer. Thick BCB is spun on this wafer and the device is glued upside down and cured at 250 °C for 1 h in N_2 ambient.

The growth substrate is removed by spray etching in NH_4OH:H_2O_2 solution and the AlAs etch stop layer is removed by dipping the sample in BHF for 20 s. The bottom QW is etched away in areas under the top ohmic contact. The samples are then cleaved on both sides to expose the waveguides. The only difference between device 2 and other devices is the way the rib of the rib waveguide is defined. For devices 1A and 1B the optical waveguides are defined with electron beam lithography and etching. First a 60-nm-thick Ti is evaporated and lifted off to be used as the etch mask. Next, the waveguides are etched to form the index loading layer with citric acid:H_2O_2 (4:1). The Ti etch mask is removed in BHF. The rest of the process steps are identical. For device 1B, all steps are identical except for the fact that ohmic metallization is switched. Fabricated devices included 7 mm phase modulators and Mach–Zehnder intensity modulators with 4 and 7 mm electrode lengths.

IV. Results and Discussion

Fig. 5 shows the current–voltage (*I–V*) and capacitance–voltage (*C–V*) measurements of a 7 mm phase modulator from device 1A. *I–V* measurement shows the expected diode characteristics. The observed behavior of the *C–V* measurement can be explained as follows. As the *p-i-n* junction is reverse biased, there is a small decrease in capacitance up to –0.7 V. Beyond this point, capacitance decreases rapidly and levels out near –2.5 V. The initial slow decrease in capacitance with voltage is due to vertical depletion of the QWs and the onset of the rapid reduction is due to depletion in the lateral direction. This reduces the lateral extend; hence, the overlap of the buried electrodes and capacitance decreases rapidly. Finally, when there is no vertical overlap between the charges in the QWs only a weak electric field overlaps with the optical mode and modulation efficiency drops precipitously. The maximum bias that can be applied for modulation without completely depleting the buried electrodes is about –2.5 V when doped QWs deplete and modulation stops. Forward bias voltages up to 1 V can also be applied. This reduces the strong built in field as evidenced by capacitance drop and produces modulation.

Optical measurements are made by end-fire coupling light from a 1550 nm DFB laser into the device and collecting light with an objective lens on to a photodetector. An iris is placed in front of the detector to filter out stray light. Fig. 7 shows the transmission of phase modulators out of devices 1A and B with 7 mm electrodes as a function of the applied voltage. The only difference between these two devices is the order of p and n electrodes as seen in Table I. Changing this order changes the direction of the vertical electric field and the sign of the LEO contribution to the index change. So, for one device LEO index change adds to the index change related to free carriers and very efficient modulation results. For the other device these

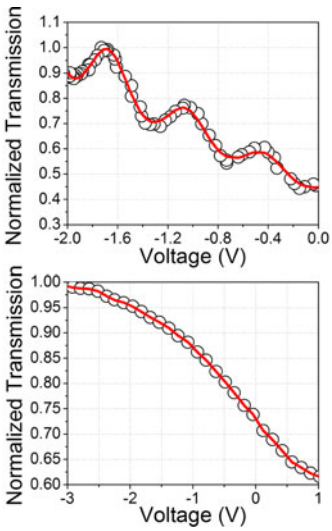

Fig. 7. Transmission of phase modulator with 7 mm electrodes as a function of bias for (a) device 1 A and (b) device 1B. $\lambda = 1.55\,\mu\mathrm{m}$. Open squares are data points and solid line is the curve fit using (6).

two contributions subtract and the modulation efficiency drops significantly. This was predicted in the modeling presented in Fig. 3 and is clearly observed in the experimental result presented in Fig. 7. In Fig. 7(a) LEO effect adds to other effects and modulation is very efficient. In Fig. 7(b) opposite occurs and modulation efficiency drops sharply. The same effect is also observed for devices fabricated in the same epilayer when waveguide orientation is rotated 90. This also changes the sign of the LEO effect. Therefore, waveguide orientation should be carefully chosen to observe the most efficient modulation. The change in the transmission is mainly due to decrease in the free carrier absorption loss resulting from carrier depletion under reverse bias. Fig. 6 shows the variation of free carrier absorption loss as a function of reverse bias for different QW doping levels. Change in the free carrier absorption loss is linear and is $\sim$ 1.7 dB/(cm·V) for the doping range covered. The results shown in Fig. 7 are curve fitted to the well-known Fabry–Perot transmission equation given as

$$T = C\frac{(1-R)^2 e^{-2\alpha l}}{(1-Re^{-2\alpha l})^2 + 4Re^{-2\alpha l}\sin^2(\phi_0 + \pi V/V_\pi)} \quad (6)$$

where R is the facet reflectivity, V_π is the drive voltage that creates π phase shift, V is the applied voltage, C and ϕ_0 are arbitrary amplitude and phase. The facet reflectivity of such compact waveguides could be very different from the regular Fresnel reflectivity [15]. For this fitting we used $R = 0.35$ which is calculated using 3-D finite difference time domain method. αl is the total optical loss and is modeled as

$$\alpha l = \alpha_0 l - \Delta\alpha_v V L. \quad (7)$$

In this expression, α_0 is the zero bias optical propagation loss coefficient, $\Delta\alpha_v$ is the differential free carrier loss coefficient, l and L are the total device and electrode length, respectively. This linear fit for loss variation due to carrier depletion is in accordance with the result shown in Fig. 6. The described curve fit yields $\alpha_0 = 10.6\,\mathrm{dB/cm}$, $\Delta\alpha_v = 1.7\,\mathrm{dB/(V\cdot cm)}$,

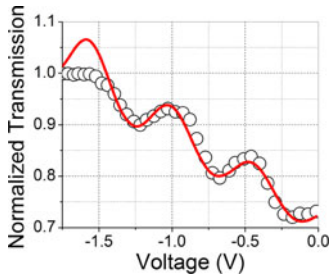

Fig. 8. Transmission of phase modulator with 7 mm electrodes as a function of bias for device 2. $\lambda = 1.55\,\mu\mathrm{m}$. Open squares are data points and solid line is the curve fit using (6).

$V_\pi = 0.62\,\mathrm{V}$ for device 1A. The corresponding values for device 1B are $\alpha_0 = 13.2\,\mathrm{dB/cm}, \Delta\alpha_v = 0.8\,\mathrm{dB/(V\cdot cm)}$, and $V_\pi = 4.9\,\mathrm{V}$. The variation in the loss values is mainly due to the difficulty of fitting device 1B data to the expected Fabry–Perot transmission. Since modulation is very inefficient there are no clear Fabry–Perot fringes and the fit is somewhat ambiguous. The main observation is the inefficient modulation. Similar measurements are made on device 2 and shown in Fig. 8.

The same fitting approach yielded $\alpha_0 = 8\,\mathrm{dB/cm}, \Delta\alpha_v = 1.4\,\mathrm{dB/(V\cdot cm)}$, and $V_\pi = 0.57\,\mathrm{V}$ for device 3. This device had lower n and p doping. In this case, modulation stops earlier due to lower doping. V_π is also slightly lower because of increased overlap factors due to higher silicon index used to define the rib waveguide. Although a single V_π is quoted, V_π shows some slight bias dependence. As reverse bias increases vertical carrier depletion increases electrode gap and V_π.

Other effects contributing to the propagation loss of the phase modulators are absorption in bulk materials and scattering from interfaces and sidewalls. We carried out a very careful study of the propagation loss in such compact waveguides [15]. Loss due to material absorption in undoped GaAs and $Al_{0.5}Ga_{0.5}As$ at 1.55 μm is very low. In such waveguides propagation loss shows very strong dependence on the roughness of interfaces and sidewalls. Interfaces are usually very smooth and sidewall roughness is the main contributor. We were able to reduce sidewall roughness of the ribs using electron beam lithography and Si liftoff. Such undoped waveguides had measured propagation loss values around 1 dB/cm [15]. Etched rib sidewalls have more roughness and higher propagation loss.

The loss values reported for the phase modulators in this study are higher. The main reason was found to be the pitting of the $Al_{0.5}Ga_{0.5}As$ surface by a stripper used in the fabrication. This interface roughness, which was discovered after fabrication was done, was absent in the devices reported in [15] and is the main reason for increased propagation loss. Another significant loss component is the coupling loss. Coupling in and out of such compact waveguide is challenging. In our study using antireflection coatings and careful alignment, we are able to keep this loss around 5 dB/facet. However, this loss can be reduced significantly using mode transformers that do not require regrowth. Since high index substrate is removed, mode transformation from the semiconductor waveguide into a much bigger polymer waveguide is possible. Although not reported here simulations

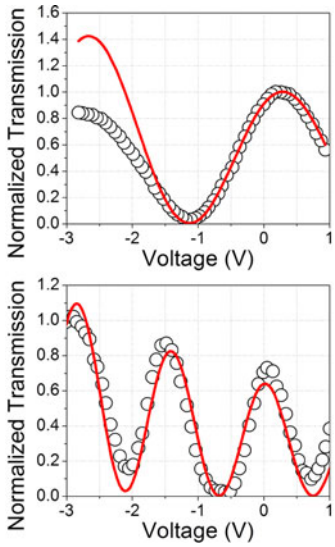

Fig. 9. Optical transmission as a function of voltage for Mach–Zehnder intensity modulators with (a) 4 mm and (b) 7 mm electrode length under single arm drive (Device 1 A). Wavelength is 1.55 μm.

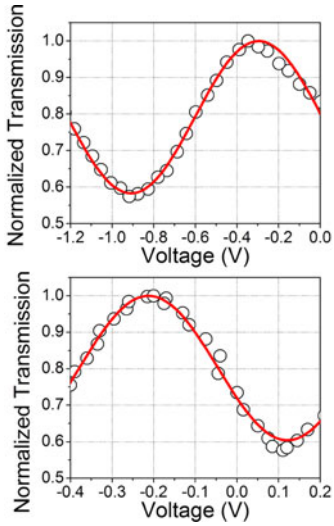

Fig. 10. Normalized transmission of Mach–Zehnder intensity modulator made out of device 2 with 7-mm-long electrodes. (a) single arm drive and (b) quasi-push–pull drive. Open circles and solid show data points and its curve fit using (8), respectively.

of such transformers indicate coupling loss can be reduced to about 1 dB/facet level. Hence, with careful processing and appropriate mode transformers insertion loss of such modulators can be kept around 5 dB.

Fig. 9 shows the transmission of Mach–Zehnder modulators out of device 1A for two different electrode lengths when only one arm of the device is driven. Very efficient amplitude modulation is evident. The 7-mm-long device goes through more than 5 maximum–minimum transmission over a 4 V voltage change. There is also increase in transmission due to absorption loss decrease originating from carrier depletion under bias. For reverse bias values exceeding 2.5 V modulation efficiency drops significantly due to depletion of buried electrodes. The measured results are curve fitted to the following equation:

$$\frac{P_{\text{out}}}{P_{\text{in}}} = \mathrm{e}^{-(2\alpha_0+\Delta\alpha_1)L}\left(\begin{array}{l}\cosh^2\left(\frac{\Delta\alpha_1 L}{2}\right)\cos^2\left(\frac{\pi}{2}\frac{V}{V_\pi}+\varphi_0\right)\\ +\sinh^2\left(\frac{\Delta\alpha_1 L}{2}\right)\sin^2\left(\frac{\pi}{2}\frac{V}{V_\pi}+\varphi_0\right)\end{array}\right). \tag{8}$$

This equation describes the normalized transmission of a Mach–Zehnder modulator when there is optical loss difference between the arms. In our case, this loss difference originates due to carrier depletion when one of the arms is biased. In this equation, V_π is the drive voltage of the modulator, L is length of the electrode, α_0 and $\Delta\alpha_1$ are the optical loss coefficient at zero bias and differential loss coefficient between the arms, and φ_0 is the phase difference between the arm at zero bias. The drive voltage of Mach–Zehnder modulators with 4 and 7 mm length electrodes are 1.41 and 0.68 V, which correspond to a drive voltage length product of 0.56 and 0.48 V·cm. These values are very close to the value obtained from Fabry–Perot phase modulator measurements.

The arms of these devices can be biased independently. Even though both arms can be biased independently true push–pull operation is not possible since reversing the bias voltage polarity would forward bias one of the arms. However a quasi-push–pull scheme can be utilized by applying $V_B + V$ to one arm and $V_B - V$ to the other, where V_B is a fixed bias voltage and V is the modulating voltage. If $|V_B| \geq |V_{\text{Peak}}|$ the reverse bias across the arms will swing between $V_B + V_{\text{Peak}}$ and $V_B - V_{\text{Peak}}$. Therefore, the voltage swing across one arm will be $2V_{\text{Peak}}$. Furthermore, when the voltage across one arm increases the voltage across the other arm decreases and neither arm is forward biased. Therefore, the required modulating voltage amplitude is reduced by a factor of two as in true push–pull operation. The result of such a measurement for device 2 is shown in Fig. 10(a) and (b). Based curve fitting to (8) the drive voltage under a single arm drive and quasi push–pull drive were found as 0.6 $\pm$ 0.1 and 0.3 $\pm$ 0.05 V, respectively. This corresponds to drive voltage length product of 0.42 $\pm$ 0.07 and 0.21 $\pm$ 0.03 V·cm, respectively. These are the lowest drive voltages reported for a bulk compound semiconductor electro-optic modulator.

Although this biasing scheme assures that there is no current injection, push–pull operation under zero bias is a possibility for low V_π devices. This is possible because forward bias up to 1 V can be applied without current injection. For example Fig. 9(b) shows that this device can be driven push pull under zero bias. However, bias helps to reduce the propagation loss and may be needed to counter the built-in arm unbalance.

For device 2, the extinction ratio (*ER*) is low mainly due unmodulated light trapped in BCB between the epilayer and transfer substrate. Although this part is not a waveguide and cannot guide radiation, index difference between the BCB and substrate/epilayer is so large that leakage is not complete. As a result some portion of the light that couples to this part emerges at the output and increases the off state power since it is not

modulated. *ER* is much better for device 1A mainly due to a thin metal layer on the surface of the transfer substrate. This layer absorbs most of this stray light. The same result can be obtained by improving the coupling using a mode transformer or intentionally misaligning the input and output waveguides. But differential loss between the arms due to carrier depletion can limit the *ER*. In the presence of this limitation, *ER* can be found using (8) as

$$ER = \frac{\left(\frac{P_{\text{out}}}{P_{\text{in}}}\right)_{\max}}{\left(\frac{P_{\text{out}}}{P_{\text{in}}}\right)_{\min}} = \left(\frac{\cosh\left(\frac{\Delta\alpha_1 L}{2}\right)}{\sinh\left(\frac{\Delta\alpha_1 L}{2}\right)}\right)^2 = \left(\frac{e^{\Delta\alpha_1 L}+1}{e^{\Delta\alpha_1 L}-1}\right)^2. \tag{9}$$

Power imbalance between the arms due to differential free carrier absorption loss is about $1.7\ \text{dB}/(\text{cm}\cdot\text{V}) \times 0.42\text{V}\cdot\text{cm} \sim 0.7\ \text{dB}$, which yields an extinction ratio of about 22.5 dB. So such a small differential loss modulation between the arms should not degrade the extinction ratio. The measured extinction ratio for device 1A was 15 dB. The additional degradation is mainly due incomplete absorption of unmodulated light trapped in BCB.

Although this technology can deliver very low drive voltages, devices presented here are not suitable for wide bandwidth operation. This is mainly due to large device capacitance and the excessive resistance of p-layer. This difficulty can be solved using a so called staircase waveguide and an *n-i-p-i-n* epilayer design [16], [17]. Modulator electrodes fabricated this way demonstrated that modulation bandwidth in excess of 35 GHz is possible for 2-mm-long electrodes. Furthermore, Mach–Zehnder intensity modulators using staircase waveguides and *n-i-p-i-n* epilayers containing MQW cores in InP system demonstrated 0.36 V·cm drive voltage length products for series connected arms [18]. Therefore, this approach has potential of delivering wide bandwidth sub volt electro-optic intensity modulators.

V. Conclusion

This study reported ultralow drive voltage Mach–Zehnder modulators with drive voltages as low as 0.3 V at 1.55 μm. This corresponds to 0.21 V·cm modulation efficiency, which is a world record for compound semiconductor bulk electro-optic modulators [8]. These modulators use highly confined substrate removed GaAs/AlGaAs optical guides with buried doped QW electrodes. Separation between the doped QW electrodes, which is the electrode gap, is only 0.15 μm. This allows the creation of very large modulating fields with very low external voltages. Such large fields create large index changes due to LEO effect and carrier depletion. A thorough analysis indicates that these index changes are almost equal and carrier depletion effects contribute strongly to modulation. Furthermore, very strong optical confinement improves the optical overlap hence large material index changes can be utilized very efficiently. However, attention should be paid to align the modulating electric field direction with respect to the crystal orientation so that LEO effect and carrier depletion effects add. This can be done using the correct waveguide orientation. Otherwise, they may subtract and very poor modulation can result since these effects are comparable. Due to depletion of buried electrodes modulating voltages can be applied up to a certain limit and modulation stops once the buried electrodes deplete. But due to very low drive voltage this is not a concern and modulation over 5 V_π range has been observed. The propagation loss of the waveguides depends on bias and reduces with applied reverse bias due to depletion. The loss dependence on bias is found to be linear based on modeling. Experimental data also support this observation. Other loss component due to scattering strongly depends on sidewall and interface smoothness and attention should be paid not to get process induced damage. Even with some process induced damage propagation loss values less than 8 dB/cm were observed. Carrier depletion related loss changes also introduce a differential loss between the arms of the Mach–Zehnder modulator. Effect of this differential loss on the *ER* was also investigated and the limit on *ER* based on experimental data was found to be about 22.5 dB. This is higher than the measured *ER* of about 15 dB. Unmodulated light trapped between the epilayer and transfer substrate in BCB was identified to be the factor limiting *ER*. Ways to eliminate this light have been proposed. These findings along with recently reported electrode designs for wide bandwidth operation make this technology a viable approach for high performance optical modulation.

References

[1] N. Dagli, "Wide bandwidth lasers and modulators for RF photonics," *IEEE Trans. Microw. Theory Tech.*, vol. MTT-47, no. 7, pp. 1151–1171, Jul. 1999.

[2] S. S. Lee, R. V. Ramaswamy, and V. S. Sundaram, "Analysis and design of high-speed high-efficiency GaAs-AlGaAs double-heterostructure wave-guide phase modulator," *IEEE J. Quantum Electron.*, vol. 27, no. 3, pp. 726–736, Mar. 1991.

[3] A. Alping, X. S. Wu, and L. A. Coldren, "Wavelength dependence of high performance AlGaAs/GaAs waveguide phase modulators," *Electron. Lett.*, vol. 23, pp. 93–95, 1987.

[4] K. Tsuzuki, T. Ishibashi, T. Ito, S. Oku, Y. Shibata, T. Ito, R. Iga, Y. Kondo, and Y. Tohmori, "A 40-Gb/s InGaAlAs-InAlAs MQW n-i-n Mach-Zehnder modulator with a drive voltage of 2.3 V," *IEEE Photon. Technol. Lett.*, vol. 17, no. 1, pp. 46–48, Jan. 2005.

[5] S. Akiyama, H. Itoh, T. Takeuchi, A. Kuramata, and T. Yamamoto, "Wide-wavelength-band (30 nm) 10-Gb/s operation of InP-based Mach-Zehnder modulator with constant driving voltage of 2 V-pp," *IEEE Photon. Technol. Lett.*, vol. 17, no. 7, pp. 1408–1410, Jul. 2005.

[6] C. Rolland, R. S. Moore, F. Shepherd, and G. Hillier, "10 Gbit/S, 1.56 μm multiquantum-well InP/InGaAsP Mach–Zehnder optical modulator," *Electron. Lett.*, vol. 29, pp. 471–472, Mar. 4, 1993.

[7] S. Nishimura, H. Inoue, H. Sano, and K. Ishida, "Electrooptic effects in an InGaAs/InAlAs multiquantum well structure," *IEEE Photon. Technol. Lett.*, vol. 4, no. 10, pp. 1123–1126, Oct. 1992.

[8] J. Shin, Y.-C. Chang, and N. Dagli, "0.3 V drive voltage GaAs/AlGaAs substrate removed mach-zehnder intensity modulators," *Appl. Phys. Lett.*, vol. 92, 201103-1–3, 2008.

[9] S. S. Lee, R. V. Ramaswamy, and V. S. Sundaram, "Analysis and design of high-speed high-efficiency GaAs-AlGaAs double-heterostructure wave-guide phase modulator," *IEEE J. Quantum Electron.*, vol. 27, no. 3, pp. 726–736, Mar. 1991.

[10] J. G. Mendoza Alvarez, L. A. Coldren, A. Alping, R. H. Yan, T. Hausken, K. Lee, and K. Pedrotti, "Analysis of depletion edge translation lightwave modulators," *J. Lightw. Technol.*, vol. 6, pp. 793–808, Jun 1988.

[11] J. Faist and F. K. Reinhart, "Phase modulation in GaAs AlGaAs double heterostructures—Part1: Theory," *J. Appl. Phys.*, vol. 67, pp. 6998–7005, Jun. 1, 1990.

[12] J. Faist and F. K. Reinhart, "Phase modulation in GaAs AlGaAs double heterostructures—Part2: Experiment," *J. Appl. Phys.*, vol. 67, pp. 7006–7012, Jun. 1, 1990.

[13] C. A. Berseth, C. Wuethrich, and F. K. Reinhart, "The electrooptic coefficients of GaAs: Measurements at 1.32 μm and 1.52 μm and study of their dispersion between 0.9 and 10 μm," *J. Appl. Phys.*, vol. 71, pp. 2821–2825, Mar. 15, 1992.
[14] D. F. Nelson and E. H. Turner, "Electro-optic and piezoelectric coefficients and refractive index of gallium phosphide," *J. Appl. Phys.*, vol. 39, pp. 3337–3343, 1968.
[15] J. Shin, Y.-C. Chang, and N. Dagli, "Propagation loss study of very compact GaAs/AlGaAs substrate removed waveguides," *Opt. Exp.*, vol. 17, no. 5, pp. 3390–3395, Mar. 2, 2009.
[16] S. Dogru and N. Dagli, "Traveling wave electrodes for wide-bandwidth substrate-removed electro-optic modulators'," in *Proc. IEEE Photon. Soc. Annu. Meeting*, Burlingame, CA, Sep. 23–27, 2012, Paper MS-5.
[17] S. Dogru, J. Shin, and N. Dagli, "Novel electrodes for wide-bandwidth substrate-removed electro-optic modulators," *OSA Opt. Lett.*, vol. 38, no. 6, pp. 914–916, 15 Mar. 2013.
[18] S. Dogru, J. Shin, and N. Dagli, "InGaAlAs/InAlAs multi quantum well substrate removed electro-optic modulators," in *Proc. IEEE Photon. Soc. Annu. Meeting*, Arlington, VA, 9–13 Oct. 2011, pp. 739–740, Paper ThJ2.

Jae Hyuk Shin (M'05) was born in Seoul, Korea. He received the B.S. degree in inorganic materials engineering from Seoul National University, Seoul, Korea, in 1999, and the Ph.D. degree in materials from the University of California at Santa Barbara, Santa Barbara, CA, USA, in 2007.

He was a Postdoctoral Researcher at the Department of Electrical and Computer Engineering, University of California at Santa Barbara till 2009. He is currently with Aurrion, Inc, Goleta, CA, USA. His research interests include the design, simulation, fabrication, and analysis of high-bandwidth low-drive voltage modulators for fiber-optic communications.

Nadir Dagli (F'06) received the Ph.D. degree in electrical engineering from Massachusetts Institute of Technology, Cambridge, MA, USA, in 1986.

After graduation he joined the Department of Electrical and Computer Engineering, University of California at Santa Barbara, Santa Barbara, CA, USA, where he is currently a Professor. His research interests include design, fabrication, and modeling of guided-wave components for optical integrated circuits, ultrafast electro-optic modulators, WDM components, and photonic nanostructures.

Dr. Dagli served and chaired many technical program and other professional committees. He was the Editor-in-Chief of IEEE PHOTONICS TECHNOLOGY LETTERS (2000–2005) and an elected member of the IEEE-LEOS board of governors (2003-2005).